Origin of tropospheric NOx over subarctic eastern Canada in summer

Origin of tropospheric NO_x over subarctic eastern Canada in summer

S.-M. Fan,[1] D.J. Jacob,[1] D.L. Mauzerall,[1] J.D. Bradshaw,[2] S.T. Sandholm,[2] D.R. Blake,[3] H.B. Singh,[4] R.W. Talbot,[5] G.L. Gregory,[6] and G.W. Sachse[6]

Abstract. The origin of NO_x in the summertime troposphere over subarctic eastern Canada is investigated by photochemical modeling of aircraft and ground-based measurements from the Arctic Boundary Layer Expedition (ABLE 3B). It is found that decomposition of peroxyacetyl nitrate (PAN) can account for most of the NO_x observed between the surface and 6.2 km altitude (aircraft ceiling). Forest fires represent the principal source of PAN in the region, implying the same origin for NO_x. There is, however, evidence for an unidentified source of NO_x in occasional air masses subsiding from the upper troposphere. Isoprene emissions from boreal forests maintain high NO_x concentrations in the continental boundary layer over eastern Canada by scavenging OH and NO_3, thus slowing down conversion of NO_x to HNO_3, both in the daytime and at night. This effect is partly compensated by the production of CH_3CO_3 radicals during isoprene oxidation, which slows down the decomposition of PAN subsiding from the free troposphere. The peroxy radical concentrations estimated from concurrent measurements of NO and NO_2 concentrations during ABLE 3B are consistent with values computed from our photochemical model below 4 km, but model values are low at higher altitudes. The discrepancy may reflect either a missing radical source in the model or interferences in the NO_2 measurement.

1. Introduction

Nitrogen oxides (NO_x = NO + NO_2) control the tropospheric production of O_3 and OH. Knowledge of the processes that govern tropospheric NO_x concentrations is essential to understanding the present, past and future oxidizing capacity of Earth's atmosphere [*Isaksen and Hov*, 1987; *Crutzen and Zimmermann*, 1991; *Thompson*, 1992]. Distributions of NO_x in the global troposphere have been simulated using two or three-dimensional chemistry, transport, and deposition models and estimated inventories of NO_x emissions [*Levy and Moxim*, 1987; *Penner et al.*, 1991; *Ehhalt et al.*, 1992; *Kasibhatla et al.*, 1993]. However, the origin of NO_x in the remote troposphere remains uncertain. Transport of primary NO_x from source regions is limited, because NO_x is oxidized to HNO_3 in a matter of a few days. It appears that diffuse chemical sources must be responsible for maintaining the NO_x levels in the remote troposphere.

Peroxyacetyl nitrate (PAN, $CH_3C(O)OONO_2$), which is produced in the oxidation of hydrocarbons, represents an ubiquitous

[1] Division of Applied Sciences, Harvard University, Cambridge, Massachusetts.
[2] School of Earth and Atmospheric Sciences, Georgia Institute of Technology, Atlanta.
[3] Department of Chemistry, University of California, Irvine.
[4] NASA Ames Research Center, Moffet Field, California.
[5] Complex Systems Research Center, University of New Hampshire, Durham.
[6] NASA Langley Research Center, Hampton, Virginia.

reservoir of NO_x in the remote troposphere [*Singh et al.*, 1986, 1990, 1992, 1994a]. Since PAN is stable at the low temperatures of the upper troposphere, it may provide a vehicle for the long-range transport of NO_x from source regions [*Crutzen*, 1979; *Singh and Hanst*, 1981]. The importance of PAN decomposition as a source of NO_x in the remote troposphere has been evaluated recently in photochemical model analyses of observations taken over western Alaska in summer (Arctic Boundary Layer Expedition (ABLE) 3A) and at Mauna Loa, Hawaii (Mauna Loa Observatory Photochemistry Experiment (MLOPEX)). *Jacob et al.* [1992] found that PAN decomposition in ABLE 3A could account for most of the NO_x observed below 4 km but not above. *Liu et al.* [1992] and *Walega et al.* [1992] found that PAN decomposition could provide only a minor source of NO_x in MLOPEX. The origin of NO_x in MLOPEX remains unclear (R. B. Chatfield, The anomolus HNO_3/NO_x ratio of remote tropospheric air: Is there conversion of nitric acid to formic acid and NO_x?, submitted to *Geophysical Research Letters*, 1994).

We present here a photochemical investigation of the NO_x budget in the troposphere over eastern Canada in summer, using data from the ABLE 3B expedition conducted in July-August, 1990 [*Harriss et al.*, 1994]. This expedition offered a comprehensive documentation of air chemistry over the region including mixing ratios of O_3, NO, NO_2, PAN, NO_y, CO, and hydrocarbons measured from aircraft up to 6.2 km altitude and biosphere-atmosphere exchange fluxes measured from an instrumented tower at a boreal woodland site near Schefferville, Quebec (see special section "The Northern Wetlands Study and the Arctic Boundary Layer Expedition 3B: An International and Interdisciplinary Field Campaign" in *Journal of Geophysical Research*, 99 (D1), 1421-1953, 1994). We analyze the origin of NO_x in ABLE 3B by using a combination of zero-dimensional (0-D) and one-dimensional (1-D) models constrained with the observations (details presented in section 2). The 0-d model calculations are used for the free tro-

FAN ET AL.: ORIGIN OF NO_x IN SUMMERTIME TROPOSPHERE

posphere, yielding an ensemble of snapshots of local photochemistry along the aircraft flight tracks from which regional statistics for the NO_x budget can be obtained. The 1-D model calculations are used for the continental boundary layer (CBL) over the boreal woodland and account for diel variations in vertical mixing and biogenic isoprene emissions. The woodlands of eastern Canada are large sources of isoprene [Blake et al., 1994]. The ABLE 3B data provide a rare chance to study the chemistry of isoprene under the low NO_x conditions which are characteristic of the CBL over remote regions.

The NO_x budgets in the free troposphere and in the continental boundary layer are presented in sections 3 and 4, respectively. Conclusions are in section 5. The appendix provides discussion on the feasibility of using the concurrent measurements of NO and NO_2 in ABLE 3B to calculate the concentration of peroxy radicals and test the accuracy of photochemical models.

2. Methods

A map of the ABLE 3B region is shown in Figure 1. Air masses of various chemical compositions were encountered by the aircraft, reflecting influences from forest and tundra fires, industrial and urban pollution, stratospheric intrusions, and tropical outflow (Table 1). The ABLE 3B mission design placed particular emphasis on sampling biomass fire plumes. Air masses influenced by biomass fire emissions, as diagnosed by CO concentrations greater than 120 ppb [Talbot et al., 1994], accounted for about 30% of the aircraft observations in the free troposphere. Lidar measurements of aerosol concentrations in the 2 to 6 km column during the expedition suggest that air influenced by biomass burning occupied, on average, 13% of the free troposphere, background air, 42%, stratospherically influenced air, 35%, and other types, 12% [Browell et al., 1994].

We use a 0-D model to calculate the concentrations of radicals and other secondary species at chemical steady state in the free troposphere. The calculations are constrained with the ensemble of measurements taken aboard the aircraft including temperature,

dew point, pressure, UV radiation fluxes (zenith and nadir), and concentrations of NO, PAN, HNO_3, O_3, CO, acetone, C_{1-7} alkanes, C_{2-3} alkenes, benzene, and toluene. Measurements of NO are more reliable than those of NO_2 owing to possible interference in the NO_2 measurement (see appendix). The calculations are conducted for 3-min averaging intervals in the aircraft observations, representing the time resolution of the NO measurement. There are 165 intervals in the free troposphere (2.5-6.2 km) where concurrent measurements are available for all the above input variables except acetone. The data are sparse for acetone; missing data are filled based on the correlation between acetone and CO (Figure 2) (see also Singh et al. [1994b]).

The 0-D model is inadequate in the continental boundary layer (CBL) (below 2.5 km), where the concentrations of radicals are sensitive to the abundance of biogenic isoprene and its oxidation products [Jacob and Wofsy, 1990]. The lifetime of isoprene is only a few hours, while the carbonyls produced successively in the isoprene oxidation chain have lifetimes of a few hours to a few days. One cannot assume that the isoprene oxidation products are in local chemical steady state with the isoprene concentrations measured aboard the aircraft. We use therefore a time-dependent, 1-D model for the CBL, following Trainer et al. [1987, 1991] and Jacob and Wofsy [1988, 1990], and apply this model to simulate observations over the Schefferville tower site on August 7 when detailed measurements from the tower and from an aircraft spiral over the tower are available. The tower site is 0.5 km above sea level. The CBL in our 1-D model extends to 2.25 km above ground level, representing the afternoon maximum of mixed layer depth as measured locally from rawinsondes [Fitzjarrald and Moore, 1994]. Photochemical calculations are conducted at seven grid points (0.01, 0.1, 0.2, 0.5, 1.0, 1.5, and 2.0 km above the canopy). Vertical transport is simulated with an eddy diffusion parameterization based on local measurements of the mixed layer depth z_i and of the fluxes of momentum and sensible heat [Lamb et al., 1975]. The eddy diffusion coefficient between z_i and 2.25 km is adjusted to reproduce the observed vertical profiles of O_3 mixing ratio, resulting in a ventilation lifetime of 4.5 days for the CBL.
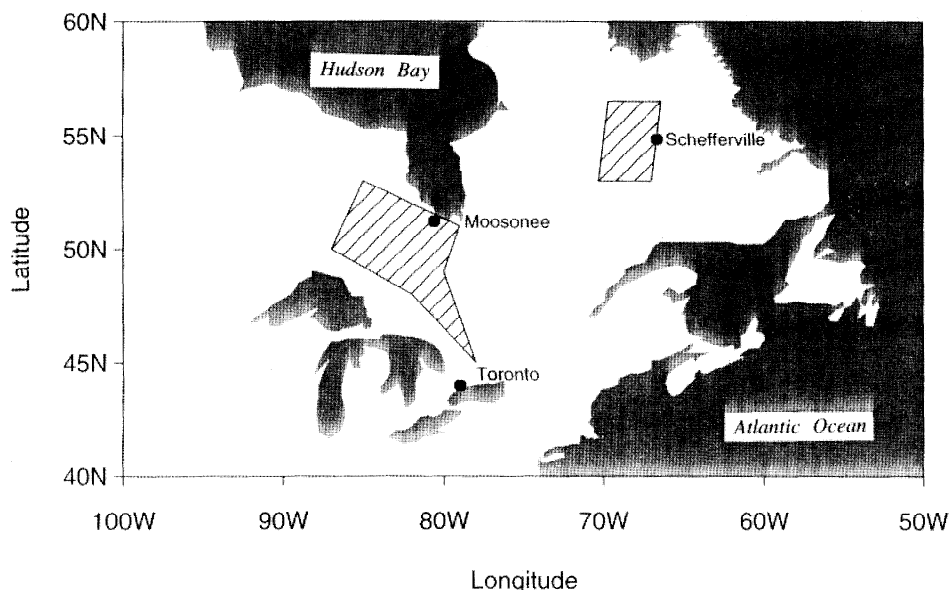

Figure 1. Map of the Arctic Boundary Layer Experiment (ABLE) 3B study region. The hatched areas indicate regions of intensive aircraft flight. The tower site was located near Schefferville, Quebec.

Table 1. Mean Characteristics of Air Masses Observed in the Free Troposphere Over Eastern Canada in Summer 1990

	Type 1, Altitude, km			Type 2, Altitude, km			Type 3, Altitude, km			Type 4, Altitude, km
	2.5-3.5	3.5-4.5	4.5-6.2	2.5-3.5	3.5-4.5	4.5-6.2	2.5-3.5	3.5-4.5	4.5-6.2	3.5-6.2
n	24	30	28	17	9	8	3	10	3	33
T, °C	-3	-6	-13	2	-6	-12	2	-3	-9	-13
DPT, °C	-8	-17	-18	-3	-13	-21	-10	-18	-17	-31
NO	6	8	7	13	13	11	7	6	8	13
NO$_2$	20	29	27	39	31	28	25	25	29	32
PAN	190	200	320	480	490	630	81	110	160	290
HNO$_3$	41	57	51	200	160	97	72	39	29	42
NO$_y$	260	510	530	900	1000	1400	110	130	230	720
O$_3$	46	54	61	58	63	66	37	37	45	61
CO	100	99	99	150	140	180	68	68	72	88
Ethyne	80	82	99	240	230	260	34	36	41	77
Ethene	24	24	39	130	110	280	20	10	10	16
Ethane	730	780	770	1100	1100	1100	440	440	520	660
Propane	59	79	93	200	190	190	22	18	28	61
Butane	10	15	16	74	63	54	5	3	3	11
Benzene	35	34	43	99	96	120	26	21	26	36
Acetone	1200	1100	1100	2100	1900	2600	560	560	640	930
ΔNO$_y$, %	2	40	22	18	32	45	-64	-36	1	47

Air mass types are defined following *Talbot et al.* [1994] as 1, Regional background; 2, biomass burning influence; 3, tropical outflow; and 4, stratospheric influence. The mean characteristics are computed from aircraft observations for the 165, 3-min intervals used in our photochemical modeling calculations. Volume mixing ratios are in parts per trillion (ppt) except for CO, O$_3$ in parts per billion. Unlisted species were generally near or below their detection limits; 10 ppt propene, 5 ppt toluene, and 2 ppt for >C$_4$ alkanes. Abbreviations are n, number of observations; T, temperature; DPT, dew point; PAN, peroxyacetyl nitrate.

ΔNO$_y$ is the percent of NO$_y$ not accounted for by observations of NO$_x$, PAN, and HNO$_3$; negative values indicate that the sum of concentrations of these species exceeded the observed concentration of NO$_y$. For further details on the NO$_y$ mass balance, see *Sandholm et al.* [1994].

The CBL model uses as upper boundary conditions the mean concentrations of O$_3$, NO, NO$_2$, and PAN measured between 2.5-3.0 km above sea level and the mean concentrations of peroxides and carbonyls calculated in the 0-D model under background conditions. Vertical profiles of HNO$_3$, CO, and hydrocarbons other than isoprene are specified using observations from the aircraft spirals below 2 km. The diurnal variations of temperature and relative humidity are specified based on interpolation of aircraft measurements and hourly ground measurements. The deposition flux of O$_3$ to the surface is calculated on the basis of the hourly mean O$_3$ deposition velocities measured at the tower, typically 0.33 cm s^{-1} during the day and 0.03 cm s^{-1} at night (J. W. Munger et al., manuscript in preparation, 1994). We assume that PAN and peroxides have the same deposition velocity as O$_3$. Soil emission of NO and dry deposition of NO$_2$ were negligibly small [*Bakwin et al.*, 1994]. The diel cycle of isoprene emission is specified according to *Jacob et al.* [1993], assuming a leaf area index of 2 and with the midday emission rate adjusted to match the isoprene concentrations measured in the CBL during the aircraft spiral. The resulting 24-hour average emission flux of isoprene is 6.1x10^{10} molecules cm^{-2} s^{-1}. In comparison, *Klinger et al.* [1994] estimated a mean isoprene emission rate of 5.5x10^{10} molecules cm^{-2} s^{-1} along a successional gradient in the Hudson Bay lowlands.

The photochemical model includes HO$_x$-NO$_x$-hydrocarbon chemistry, based on recent compilations of kinetic and product data [*Atkinson*, 1990; *Atkinson et al.*, 1992; *DeMore et al.*, 1992].

The mechanism for photochemical decomposition of isoprene follows *Tuazon and Atkinson* [1989, 1990a, b]. Nighttime isoprene chemistry follows *Paulson and Seinfeld* [1992]. Cross sections for photolysis of PAN and the rate for PAN oxidation by OH are from recent measurements (R. K. Talukdar et al., manuscript in preparation, 1994).

Aerosol chemistry is not included in our calculations. Nighttime hydrolysis of N$_2$O$_5$ in aqueous aerosols is a sink for NO$_x$ [*Heikes and Thompson*, 1983; *Dentener and Crutzen*, 1993]. However, the NH$_4^+$/SO$_4^-$ equivalent ratio in ABLE 3B averaged 1.4 for background air [*Gorzelska et al.*, 1994], implying that sulfate aerosol would be present as solid (NH$_4$)$_2$SO$_4$ [*Tang et al.*, 1978]. Conversion of N$_2$O$_5$ to HNO$_3$ on solid aerosols is negligibly slow [*Mozurkewich and Calvert*, 1988].

In the 0-D model the NO$_2$ photolysis rate coefficient J_{NO_2} is obtained from the UV measurements by zenith and nadir Eppley radiometers [*Madronich*, 1987; *Chameides et al.*, 1990]. Photolysis rate coefficients for other species are calculated using a six-stream radiative transfer model for the clear sky, Rayleigh-scattering atmosphere [*Logan et al.*, 1981] and are scaled by the ratio of J_{NO_2} calculated with the model to J_{NO_2} derived from the UV measurements. In these calculations, surface albedo is fixed at 0.06, a value obtained from extrapolation of Eppley measurements to ground level. The overhead ozone column is taken from daily satellite measurements at a resolution of 1° latitude by 1° longitude (total ozone mapping spectrometer) and ranges from 290 to 360 Dobson units. The ratio of J_{NO_2} obtained from Eppley meas-
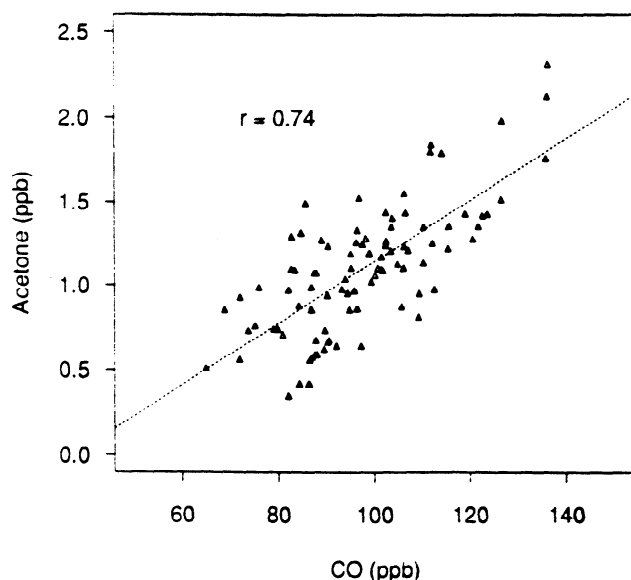
Figure 2. Relationship of acetone with CO. The line represents a least squares fit through the data. Mixing ratios of CO were averaged to measurement intervals of acetone. Data include all acetone measurements over eastern Canada during ABLE 3B.

urements to J_{NO_2} calculated from the radiative transfer model averages 1.1 (±0.2, standard deviation) under clear sky conditions (i.e., no clouds above or below the instrument). Thus the J_{NO_2} values from the UV measurements and from the radiative transfer model are consistent under the conditions where they can be compared. In the 1-D model, photolysis rates are calculated for clear sky conditions (August 7 was a clear day except for a few clouds in the morning).

3. NO_x in the Free Troposphere

Mean production and loss rates of NO_x in the free troposphere during daytime are shown in Figure 3 for individual air mass types. The reaction rates calculated for each 3-min interval were first averaged according to time of day (2-hour bins, with morning/afternoon folding to overcome a lack of measurements in the early morning) and then averaged over daytime hours (0600-1800 LT). Nighttime chemistry is assumed negligible in the free troposphere for reasons discussed above. We find that sources and sinks of NO_x are in close balance in background air (Table 1, type 1). Decomposition of PAN represents the largest source for NO_x, and therefore can explain most of the observed NO_x during ABLE 3B. Photoreduction of HNO_3 to NO_x is negligibly slow.

The effect of uncertainties in measured concentrations and rate constants must be considered in our NO_x mass balance. The rates for PAN formation and thermal decomposition are estimated to have uncertainties of 20% at 298 K [Atkinson et al., 1992]. The precision and accuracy of the PAN measurement are estimated to be 10% and 25%, respectively, of PAN mixing ratios [Singh et al., 1994a]. The principal sources of the CH_3CO_3 precursor to PAN in the model are photolysis of acetone, oxidation of acetaldehyde, and decomposition of PAN. The error caused by inferring acetone concentrations from observations of CO can be estimated to be 0.25 ppb (Figure 2), which would cause a mean error of 0.2 parts per trillion per hour (hereafter, ppt h^{-1}) in the computation of PAN production. Although the above uncertainties are substantial, they
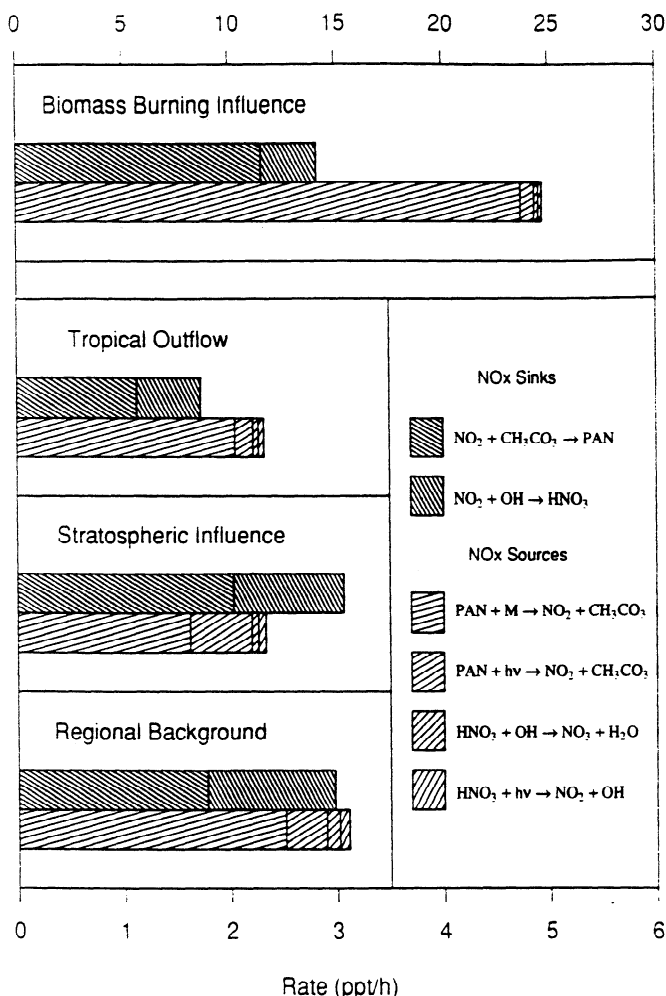

Figure 3. Sources and sinks of NO_x in the free troposphere (2.5-6.2 km) during ABLE 3B. Values are daytime means obtained by averaging the rates (parts per trillion per hour) computed for individual 3-min intervals, first according to time of day (2-hour bins, with morning/afternoon folding) and then over 12 hours from 0600 to 1800 LT. The data were segregated by air mass type (Table 1). The number of data points used in the computation are, respectively, 16: for all data, 82 for background air, 33 for stratospheric influence, 16 for tropical outflow, and 34 for biomass fire influence. The top abscissa scale is for the case of biomass burning influence, and the bottom abscissa scale is for all other cases.

are not so large as to affect our central conclusion that PAN decomposition can account for most of the NO_x observed during ABLE 3B.

Forest and tundra fires were found to be the major source for PAN, acetone, and other nonmethane hydrocarbons during ABLE 3B [Singh et al., 1994b; Talbot et al., 1994; Wofsy et al., 1994]. Long-range transport of midlatitude pollution was found to be of secondary importance. Nitrogen oxides emitted from biomass burning are efficiently converted to PAN in the fire plumes, because of the abundance of reactive hydrocarbons [Jacob et al., 1992], and additional PAN is formed on the regional scale following photolysis of pyrogenic acetone.

Air masses sensibly influenced by biomass burning in ABLE 3B (Table 1, type 2) showed indication of rapid decomposition of

PAN (Figure 3). The resulting net source for NO$_x$ in Figure 3 is 10 ppt h^{-1}, but the mean concentration of NO$_x$ in these air masses was only 40-50 parts per trillion (hereafter, ppt). Reconciling the model NO$_x$ budgets with the observed NO$_x$ concentrations would require rapid dilution of the air masses with the regional background. However, an underestimate of PAN formation is also possible, because many primary and secondary species, particularly oxygenated hydrocarbons, may be present in type 2 air masses but not included in the model. Such species could decompose to yield CH$_3$CO$_3$ radical and promote PAN formation.

Tropical air masses originating from the Pacific Ocean (Table 1, type 3) showed a near balance between chemical sources and sinks of NO$_x$ (Figure 3). However, the total NO$_y$ was exceeded by the sum of individual NO$_y$ species in these air masses. Reasons for the abnormal NO$_y$ composition are unclear; measurement errors could not be ruled out, though it is unlikely that possible errors can account for all of missing NO$_y$ [Sandholm et al., 1994].

Air masses subsiding from the upper troposphere (Table 1, type 4) represent the only case where decomposition of PAN was insufficient to account for the observed NO$_x$. One possible explanation for the missing NO$_x$ source is decomposition of unidentified nitrogen compounds. Nearly 50% of total NO$_y$ in type 4 air masses was unaccounted for by measurements of NO$_x$, PAN, and HNO$_3$ (Table 1). Figure 4 shows the relation between the net loss of NO$_x$ computed in the model, equivalent to a missing source of NO$_x$, and the NO$_y$ deficit in air of type 4. The missing source
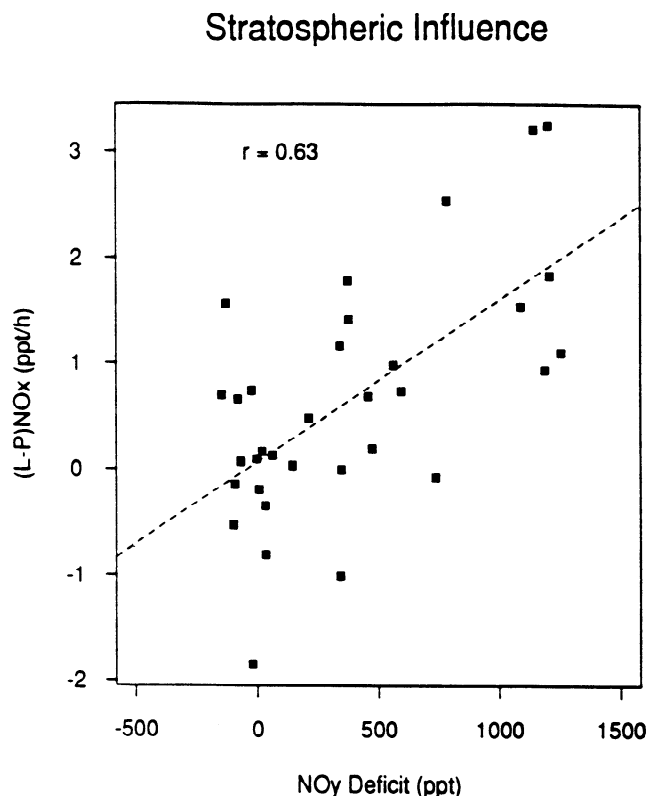
Stratospheric Influence

Figure 4. Relationship of the net chemical loss rate for NO$_x$, (L-P)NO$_x$ (parts per trillion per hour), with the NO$_y$ deficit (parts per trillion by volume) in air masses influenced by intrusions from the upper troposphere or lower stratosphere (Table 1, type 4). The NO$_y$ deficit is the difference between the measured NO$_y$ and the sum of NO$_x$, peroxyacetyl nitrate (PAN), and HNO$_3$ measured simultaneously. The line represents a least squares fit (slope = 0.00154).

of NO$_x$ appears to increase with the NO$_y$ deficit. The NO$_x$ budget would be balanced if the missing species representing the NO$_y$ deficit were converted to NO$_x$ in the free troposphere with chemical lifetime of a few weeks. A remarkable feature of air masses of type 4 was the low mixing ratio of HNO$_3$ (42 ppt on average). Such a concentration would be obtained in about 3 days from oxidation of NO$_x$ (Figure 3). Reduction of HNO$_3$ to NO$_x$ on a timescale of 3 days would balance the NO$_x$ budget (Figure 3), but the chemical lifetime of HNO$_3$ against photolysis and reaction with OH is about 2 weeks.

One way to explain the NO$_x$ and HNO$_3$ budgets as well as the missing NO$_y$ species in air masses of type 4 would be by reaction of CH$_2$O with HNO$_3$ on concentrated sulfuric acid aerosols, producing methyleneglycol nitrates (HOCH$_2$ONO$_2$, CH$_2$(ONO$_2$)$_2$) [Travagli, 1938]. Methyleneglycol nitrates have low solubility and would volatilize from the aerosols to the gas phase. They are likely photodissociated to release NO$_2$, by analogy with methyl nitrate; they would have a lifetime of the order of a few weeks. Sandholm et al. [1994] found the observed NO$_y$ deficit species to increase with O$_3$ concentration (or altitude) and to increase with the photochemical age of the air mass as measured by the CO/C$_2$H$_2$ ratio. These observations seem consistent with possible formation of HOCH$_2$ONO$_2$ and CH$_2$(ONO$_2$)$_2$ in the upper troposphere.

A comparison can be made between the NO$_x$ budgets in ABLE 3B and those in ABLE 3A. Free troposphere concentrations of NO, PAN, and O$_3$ were similar in both expeditions [Sandholm et al., 1992, 1994; Singh et al., 1992, 1994a] temperatures were also similar. Therefore we expect PAN decomposition to also have accounted for most of the NO$_x$ in ABLE 3A. In their modeling of ABLE 3A data, Jacob et al. [1992] argued that PAN decomposition could account for the NO$_x$ below about 4 km but not at higher altitudes. They used a PAN decomposition rate constant taken from Lurmann et al. [1986] that is about 30% lower than used here [Atkinson et al., 1992].

4. NO$_x$ in the Continental Boundary Layer

We now turn to an analysis of the origin of NO$_x$ in the continental boundary layer (CBL) over the boreal woodland at Schefferville using the 1-D model for August 7 described in section 2. We address the following questions. (1) Does decomposition of PAN subsiding from the free troposphere account for NO$_x$ in the CBL? (2) How does vegetative emission of isoprene affect NO$_x$ and PAN? (3) How sensitive is the NO$_x$ budget in the CBL to the RO$_2$ + HO$_2$ reactions? The last question is motivated by the lack of kinetic data for the reactions of organic peroxy radicals (RO$_2$) arising from photochemical oxidation of isoprene. Reactions of these peroxy radicals with each other are probably slow [Madronich and Calvert, 1990], but reactions with HO$_2$ may be rapid [Atkinson, 1990]. The reaction products are assumed to be organic peroxides (ROOH) which may photolyze, react with OH, or be removed by deposition. The latter two sinks would represent real loss of radicals from the atmosphere.

To address the above questions, we present here results from three simulations (1) a standard run including isoprene emission, RO$_2$ + HO$_2$ reactions with a rate constant $k = 3.4 \times 10^{-13} e^{800/T}$ cm^3 molecule^{-1} s^{-1} taken from Atkinson [1990], and ROOH photolysis at a rate twice that for CH$_3$OOH; (2) a sensitivity run with zero isoprene emission; and (3) another sensitivity run with isoprene emission but without the RO$_2$ + HO$_2$ reactions. Our definition of RO$_2$ here does not include the CH$_3$O$_2$ radicals, for which kinetic measurements of the reaction with HO$_2$ are available.

Figure 5 shows aircraft measurements of ambient temperature, absolute humidity, and mixing ratios of CO over the tower site on the afternoon of August 7. The air mass below 2 km originated from the Hudson Bay region 5 days prior to aircraft measurements and was not modified by rain or combustion emissions during the transit period [Shipham et al., 1994]. The composition of that air mass is typical of the regional background (Table 1). Tropical influence from the Pacific is apparent above 2 km and is manifested in Figure 5 by the low mixing ratios of CO (<80 ppb). This tropical influence was transitory [Shipham et al., 1994]; therefore we assume that the boundary layer had been in contact with a free troposphere of background composition in the few days before being overriden by the tropical air. This assumption dictates our choice of upper boundary conditions (section 2).

Figure 6 shows the comparisons of model mixing ratios of isoprene, O$_3$, NO, NO$_2$, and PAN with observations. The model simulates NO, NO$_2$, and PAN within the measurement uncertainties. The vertical distribution of isoprene is controlled by turbulent mixing and by OH oxidation in the boundary layer (the isoprene emission flux was adjusted to match the observed isoprene concentrations.) Concentrations of O$_3$ are controlled mainly by transport from the free troposphere and deposition. The net photochemical production of O$_3$ in the CBL is small, about 20% of the flux from the free troposphere.

The sensitivity simulation without isoprene emission yields O$_3$, NO, and NO$_2$ within the range of measurements. However, the PAN mixing ratio in the CBL falls below the measurement by a factor of more than 2. In the standard simulation, oxidation of isoprene yields high concentrations of the CH$_3$CO$_3$ radical. As a result, PAN decomposition is compensated by rapid PAN formation. Our simulation with no isoprene predicts concentrations of NO$_x$ and PAN close to observed in the CBL over Alaskan tundra during ABLE 3A [Bakwin et al., 1992; Sandholm et al., 1992; Singh et al., 1992]. Isoprene is not emitted by the major tundra plants (lichens and mosses).

The sensitivity simulation without RO$_2$ + HO$_2$ reactions yields mixing ratios of NO a factor of 2 lower than the standard simulation and significantly lower than the measurements. The afternoon mixing ratio of total peroxy radicals (ΣRO$_2$) in this simulation is higher than 100 ppt (Figure 7).

Figure 8 shows the simulated NO$_x$ and PAN budgets in the boundary layer for the standard simulation. The formation of HNO$_3$ is nearly balanced by decomposition of PAN subsiding from the free troposphere; net exchange of NO$_x$ between the CBL and the free troposphere is small. The production of HNO$_3$ occurs mostly in the daytime. At night, isoprene reacts rapidly with NO$_3$, producing isoprene nitrate radicals [Atkinson et al., 1988; Dlugokencky and Howard, 1989] which release NO$_2$ upon further reactions after sunrise [Paulson and Seinfeld, 1992]; this effectively prevents the nighttime formation of N$_2$O$_5$ and hence the loss of NO$_x$ to HNO$_3$ via N$_2$O$_5$ hydrolysis. Thus isoprene suppresses formation of HNO$_3$ by depleting OH during daytime (Figure 7) and by reacting with NO$_3$ at night. As a result, the lifetime of NO$_x$ in the CBL is considerably longer with than without isoprene, 2.9 versus 1.2 days. Loss of NO$_x$ in the former case could be more rapid than computed here if isoprene nitrate radicals react on aerosols to yield HNO$_3$.

5. Summary

The origin of NO$_x$ in the summertime subarctic troposphere over eastern Canada was studied by modeling aircraft and ground observations from the ABLE 3B expedition. It is found that decomposition of PAN can account fully for the observed NO$_x$ concentrations in the free troposphere below 6 km except in occasional air masses subsiding from the upper troposphere. There is evidence that other organic nitrates are present in these air masses, and their decomposition may provide significant sources for NO$_x$. We speculate that HNO$_3$ may react with CH$_2$O in concentrated sulfuric acid aerosols to produce HOCH$_2$ONO$_2$ and CH$_2$(ONO$_2$)$_2$ and that these nitrates would photolyze on a timescale of weeks to release NO$_x$.

Decomposition of PAN subsiding from aloft appears to provide the primary source of NO$_x$ in the continental boundary layer (CBL) over eastern Canada woodlands. The NO$_x$ budget in the CBL is strongly influenced by isoprene emission from vegetation. On the one hand, isoprene increases the lifetime of NO$_x$ in the CBL by scavenging OH in the daytime and NO$_3$ at night (the isoprene nitrate radicals produced at night are assumed to return
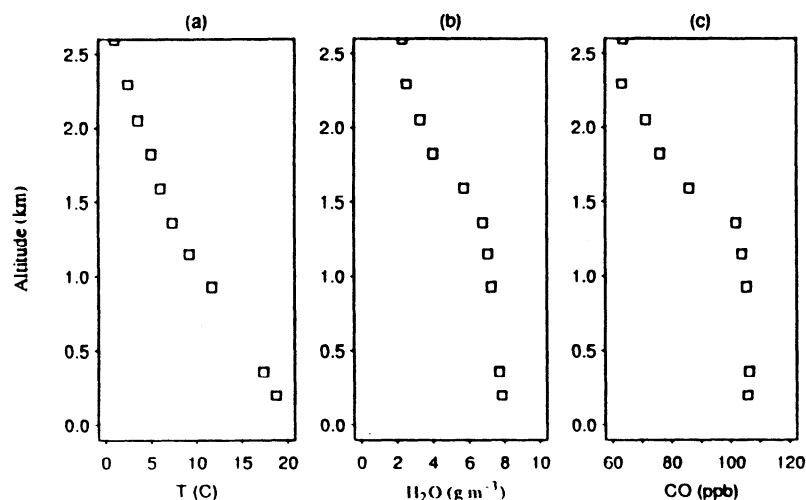

Figure 5. (a) Temperature (T) and concentrations of (b) H$_2$O and (c) CO from aircraft during a descending spiral over the Schefferville tower site at 1310-1330 LT on August 7, 1990. Each data point represents a mean measurement over a 3-min interval.
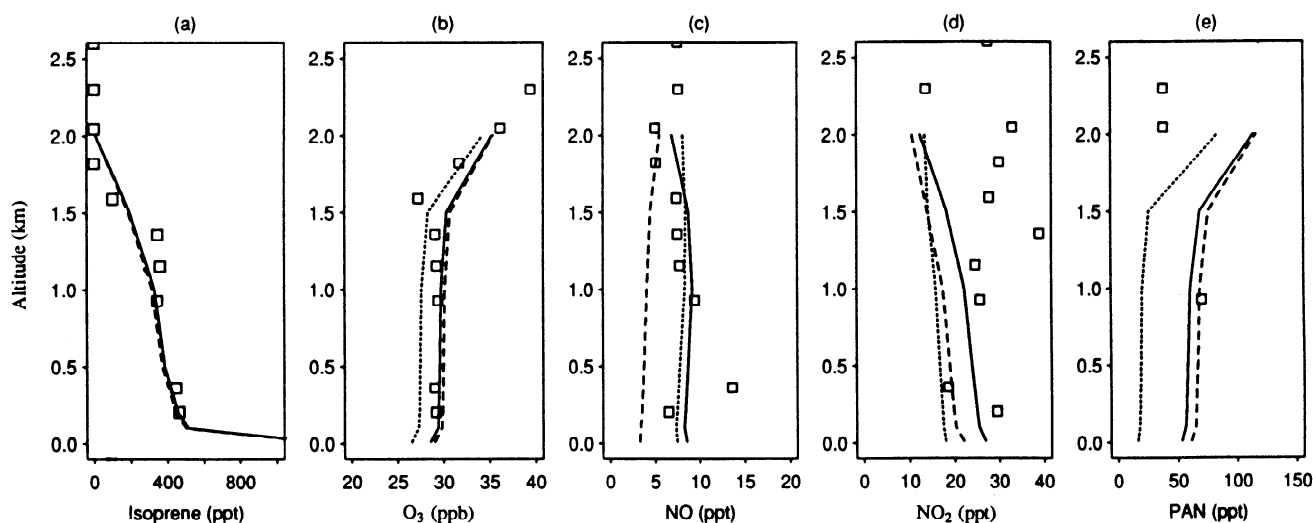
Figure 6. Comparisons of model mixing ratios of (a) isoprene, (b) O$_3$, (c) NO, (d) NO$_2$, and (e) peroxyacetyl nitrate (PAN) with measurements taken from aircraft during a descending spiral over the Schefferville tower site at 1310-1330 LT on August 7. The squares show mean measurements over 3-min intervals. The lines show model results (solid line, standard simulation; dotted line, no isoprene; and dashed line, no RO$_2$ + HO$_2$ reactions). The upper boundary conditions at 2.5 km above ground are 0 parts per trillion (ppt) isoprene, 40 ppb O$_3$, 6 ppt NO, 20 ppt NO$_2$, and 150 ppt PAN.

NO$_x$ upon sunrise). On the other hand, the production of CH$_3$CO$_3$ radicals from isoprene oxidation slows down PAN decomposition and hence the source of NO$_x$. For the conditions in ABLE 3B, the net effect of isoprene is to increase NO$_x$ concentrations in the boundary layer, providing thus a small boost for O$_3$ production.

Forest fires appeared to be the most important source for PAN during ABLE 3B. Formation of PAN occurs in fresh biomass burning plumes and also in the regional atmosphere following dispersal of pyrogenic acetone and other hydrocarbons. Subsequent transport and decomposition of PAN can then maintain a uniform distribution of NO$_x$ in the troposphere.

Appendix: Constraints on Peroxy Radicals

A critical variable in predictions of the photochemical activity of the atmosphere is the total concentration of peroxy radicals (ΣRO$_2$). Concurrent measurements of NO, NO$_2$, and O$_3$ concentrations, together with J_{NO_2}, allow, in principle, a direct computation of ΣRO$_2$ concentrations [*Ritter et al.*, 1979; *Kelly et al.*, 1980; *Parrish et al.*, 1986; *Volz et al.*, 1988; *Chameides et al.*, 1990; *Ridley et al.*, 1992; *Davis et al.*, 1993]. Rapid cycling of NO and NO$_2$ occurs in the daytime through the following reactions:
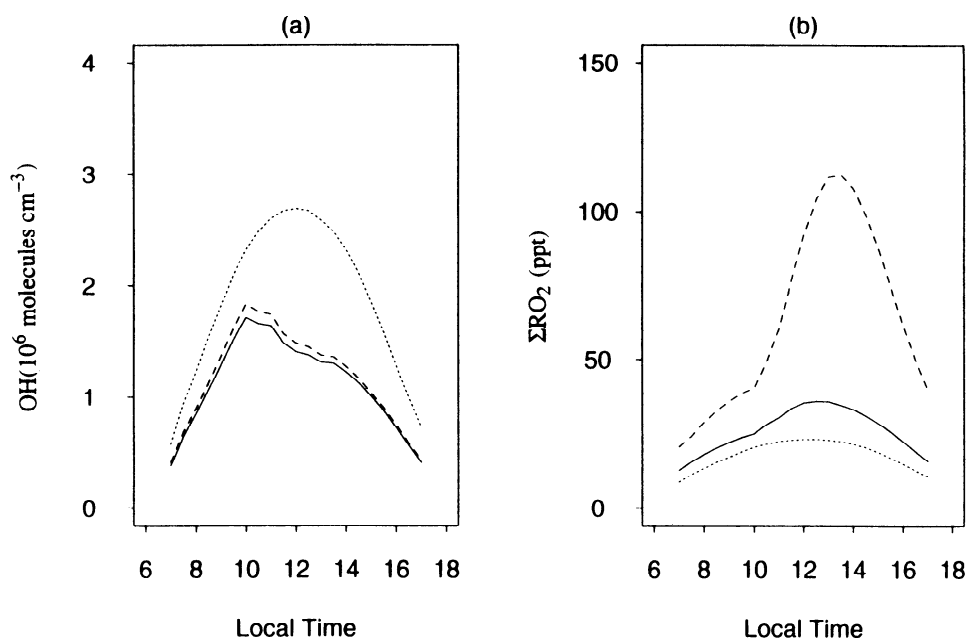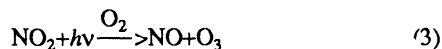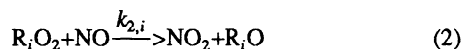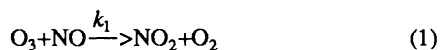

Figure 7. Concentrations of (a) OH and (b) ΣRO$_2$ (sum of peroxy radicals, values in parts per trillion) at 1.0 km above ground for the simulations described in Figure 6.

$$O_3 + NO \xrightarrow{k_1} NO_2 + O_2 \quad (1)$$

$$R_iO_2 + NO \xrightarrow{k_{2,i}} NO_2 + R_iO \quad (2)$$

$$NO_2 + h\nu \xrightarrow{O_2} NO + O_3 \quad (3)$$

where $k_{2,i}$ is the rate constant of reaction (2) for the i'th peroxy radical. Photochemical steady state between NO and NO_2 is established on a timescale of a few minutes. The steady state relation is given by

$$J_{NO_2}[NO_2] = (k_1[O_3] + \sum_i k_{2,i}[R_iO_2])[NO] \quad (4)$$

The values of $k_{2,i}$ for CH_3O_2, CH_3CO_3, and other organic peroxy radicals are within 20% of that for HO_2 for the range of observed temperatures (-30°C to 20°C) [Atkinson et al., 1992]. We choose the rate constant of the HO_2 + NO reaction, simply denoted k_2, as an approximation of $k_{2,i}$ values. We represent the sum of peroxy radicals by

$$\Sigma RO_2 = \sum_i [R_iO_2] = \frac{J_{NO_2}[NO_2]}{k_2[NO]} - \frac{k_1[O_3]}{k_2} \quad (5)$$

which may be evaluated from measurements of ambient temperature, J_{NO_2}, and concentrations of O_3, NO, and NO_2. We call this quantity "implied" ΣRO_2.

Errors for this implied ΣRO_2 may be estimated from measurement errors for the individual variables,

$$\Delta \Sigma RO_2 = \left[\frac{\Delta J_{NO_2}}{J_{NO_2}} + \frac{\Delta[NO]}{[NO]} + \frac{\Delta[NO_2]}{[NO_2]} \right] \left[\Sigma RO_2 + \frac{k_1}{k_2}[O_3] \right] \quad (6)$$

Measurement errors for O_3 are small and therefore neglected. The uncertainties on k_1 and k_2 are respectively 20 and 25% [Atkinson

et al., 1992] but are neglected as they also occur in model calculations. The values of $k_1/k_2[O_3]$ averaged 65 ppt in the free troposphere during ABLE 3B. Stated measurement precisions for 3-min averaging intervals were about 20% for NO at 10 ppt and 20% for NO_2 at 30 ppt [Sandholm et al., 1994]. Measurement uncertainties on J_{NO_2} are about 20% [Madronich, 1987; Shetter et al., 1992]. Hence a typical measurement error for the ΣRO_2 concentration would be at least 60%. Much larger errors for ΣRO_2 are expected when measured mixing ratios of NO fall below 10 ppt and NO_2 below 30 ppt, respectively. Therefore it is not instructive to compare model ΣRO_2 with the implied ΣRO_2 at 3-min averaging intervals. We reduce the uncertainty in the implied ΣRO_2 by averaging over a large number of intervals.

Figure A1 shows the implied ΣRO_2 mixing ratios as a function of NO averaged over all intervals for which data are available for constraining the model. Values of ΣRO_2 increase with decreasing NO and exceed 200 ppt for NO less than 5 ppt. Concentrations of ΣRO_2 of a few 100 ppt would result in rapid O_3 production (of the order of 1 ppb h^{-1}), which seems inconsistent with the concentrations of O_3 typically observed in the free troposphere. Further, this high level of ΣRO_2 could not be maintained by known sources of odd hydrogen radicals. On the other hand, possible unknown errors in the NO measurements have been estimated to be at or below 3.5 ppt [Sandholm et al., 1994], so the implied ΣRO_2 at a few ppt NO may not be reliable. Figure A2 compares simulated and implied mixing ratios of ΣRO_2 for the subset of data with NO above 10 ppt (i.e., x5 measurement noise). The implied ΣRO_2 mixing ratios show large variances and appear to increase with altitude. The model underpredicts the implied ΣRO_2 by a factor of 2-3 above 4 km; the discrepancy is less at lower altitudes.

The discrepancy could conceivably reflect a large missing source of odd hydrogen radicals in the model at high altitudes.
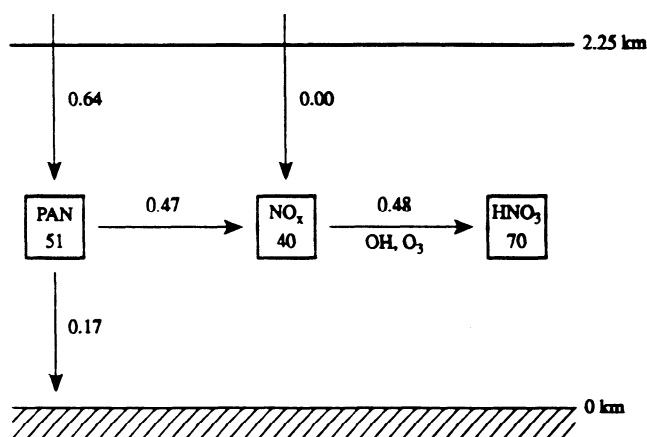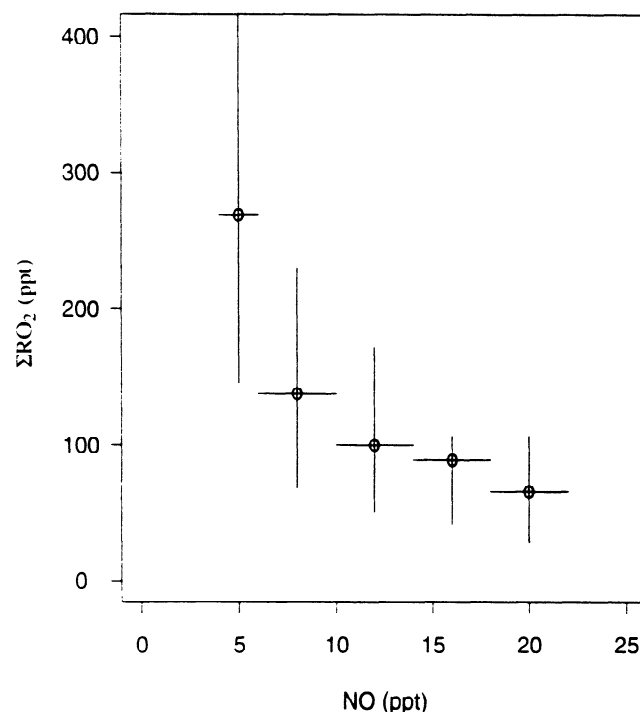

Figure 8. Diel mean budgets of NO_x and PAN computed for the boundary layer over Schefferville, Quebec. Rates (parts per trillion per hour) and concentrations (parts per trillion) are shown (note that the model specifies 70 ppt HNO_3). Exchange of NO_x with the surface is considered negligible [Bakwin et al., 1994].

Figure A1. Observed ΣRO_2 versus NO concentrations (both values in parts per trillion). The circles indicate median ΣRO_2, and vertical bars indicate quartiles for binned NO intervals shown by horizontal bars. Data between 0900 and 1500 LT and mixing ratios of NO and NO_2 above 2σ (instrumental noises) are selected.
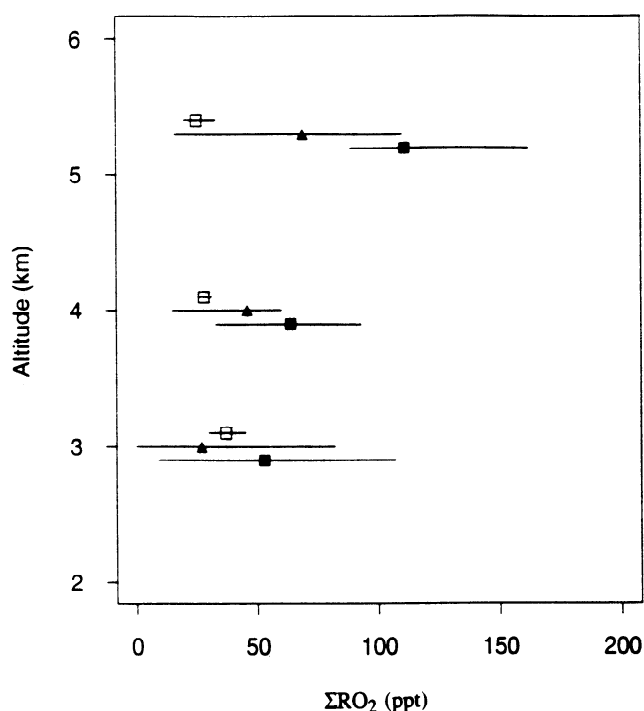
Figure A2. Median concentrations (values in parts per trillion) of peroxy radicals between 0900 and 1500 LT and in three altitude bands, 2.5-3.5, 3.5-4.5, and 4.5-6.2 km. Data are selected for NO > 10 parts per trillion. Horizontal bars indicate quartiles; solid squares, implied ΣRO_2; open squares, predicted ΣRO_2; and triangles, implied ΣRO_2 assuming that HNO_4 was measured as NO_2.

Alternatively, it is possible that interferences in NO_2 measurements, increasing with altitude, may be responsible. In particular, HNO_4 could heterogeneously decompose in the sampling tubing [Ridley et al., 1988; Sandholm et al., 1992, 1994]. Our model predicts significant levels of HNO_4 in the free troposphere, with HNO_4/NO_2 concentration ratios increasing from 0.2 at 3 km to 0.9 at 6 km, on the average. To illustrate the potential effect of an HNO_4 interference, we recalculated ΣRO_2 mixing ratios using adjusted NO_2 (which equals observed NO_2 minus simulated HNO_4). The agreement between simulated and implied mixing ratios of ΣRO_2 is somewhat improved (Figure A2). Concentrations of PAN also increased with altitude and were many times larger than those of NO_2 [Singh et al., 1994a]. If a few percent of PAN decomposed in the sampling tubing, the interference on the NO_2 measurement would be significant. For the instrument configuration used in ABLE 3B the wall reaction efficiency would need to be approximately 1 x 10^{-4} for a 50% conversion efficiency of $HNO_4 \to NO_2 + HO_2$ and 1 x 10^{-5} for a 5% conversion efficiency of PAN.

Measurements of NO are more reliable and were therefore chosen as constraint in the 0-D model calculations. Since the disagreement between implied and modeled ΣRO_2 concentrations is less at lower altitudes, we also use the NO_2 measurements as model constraints in the boundary layer calculations.

References

Atkinson, R., Gas-phase tropospheric chemistry of organic compounds: A review, Atmos. Environ., 24A, 1-41, 1990.

Atkinson, R., S.M. Aschmann, and J.N. Pitts Jr., Rate constants for the gas-phase reactions of the NO_3 radical with a series of organic compounds at 296±2K, J. Phys. Chem., 92, 3454-3457, 1988.

Atkinson, R., D.L. Baulch, R.A. Cox, R.F. Hampson, Jr., J.A. Kerr, and J. Troe, Evaluated kinetic and photochemical data for atmospheric chemistry, supplement IV, IUPAC subcommittee on gas kinetic data evaluation for atmospheric chemistry, J. Phys. Chem. Ref. Data, 21, 1125-1568, 1992.

Bakwin, P.S., S.C. Wofsy, and S.-M. Fan, Measurements of NO_x and NO_y concentrations and fluxes over Arctic tundra, J. Geophys. Res., 97, 16,545-16,557, 1992.

Bakwin, P.S., et al., Reactive nitrogen oxides and ozone above a taiga woodland, J. Geophys. Res., 99, 1927-1936, 1994.

Blake, D.R., T.W. Smith Jr., T.-Y. Chen, W.J. Whipple, and F.S. Rowland, Effects of biomass burning on summertime nonmethane hydrocarbon concentrations in the Canadian wetlands, J. Geophys. Res., 99, 1699-1719, 1994.

Browell, E.V., M.A. Fenn, C.F. Butler, W.B. Grant, R.C. Harriss, and M.C. Shipham, Ozone and aerosol distributions in the summertime troposphere over Canada, J. Geophys. Res., 99, 1739-1755, 1994.

Chameides, W.L., et al., Observed and model-calculated NO_2/NO ratios during the NASA GTE/CITE 2 field study, J. Geophys. Res., 95, 10,235-10,247, 1990.

Crutzen, P.J., The role of NO and NO_2 in the chemistry of the troposphere and stratosphere, Annu. Rev. Earth Planet. Sci., 7, 443-472, 1979.

Crutzen, P.J., and P.H. Zimmermann, The changing photochemistry of the troposphere, Tellus, 43, 136-151, 1991.

Davis, D.D., et al., A photostationary analysis of the NO_2-NO system, based on airborne observations from the subtropical/tropical north and south Atlantic, J. Geophys. Res., 98, 23,501-23,523, 1993.

DeMore, W.B., S.P. Sander, D.M. Golden, M.J. Molina, R.F. Hampson, C.E. Kolb, M.J. Kurylo, C.J. Howard, and A.R. Ravishankara, Chemical kinetics and photochemical data for use in stratospheric modeling, JPL Publ. 92-20, 1992.

Dentener, F.J., and P.J. Crutzen, Reaction of N_2O_5 on tropospheric aerosols: Impact on the global distributions of NO_x, O_3, and OH, J. Geophys. Res., 98, 7149-7163, 1993.

Dlugokencky, E.J., and C.J. Howard, Studies of NO_3 radical reactions with some atmospheric organic compounds at lower pressures, J. Phys. Chem., 93, 1091-1096, 1989.

Ehhalt, D.H., F. Rohrer, and A. Wahner, Sources and distribution of NO_x in the upper troposphere at northern midlatitudes, J. Geophys. Res., 97, 3725-3738, 1992.

Fitzjarrald, D. R., and K.E. Moore, Growing season boundary layer climate and surface exchanges in a subarctic lichen woodland, J. Geophys. Res., 99, 1899-1917, 1994.

Gorzelska, K., R.W. Talbot, K. Klemm, B. Lefer, O. Klemm, G.L. Gregory, B. Anderson, and L.A. Barrie, Chemical composition of the atmospheric aerosol in the troposphere over the Hudson Bay lowlands and Quebec-Labrador regions of Canada, J. Geophys. Res., 99, 1763-1779, 1994.

Harriss, R.C., S.C. Wofsy, J.M. Hoell Jr., R.J. Bendura, J.W. Drewry, R.J. McNeal, D. Pierce, V. Rabine, and R.L. Snell, The Arctic Boundary Layer Expedition (ABLE 3B): July - August 1990, J. Geophys. Res., 99, 1635-1643, 1994.

Heikes, B.G., and A.M. Thompson, Effects of heterogeneous processes on NO$_3$, HONO, and HNO$_3$ chemistry in the troposphere, *J. Geophys. Res., 88*, 10,883-10,895, 1983.

Isaksen, I.S.A., and O. Hov, Calculation of trends in the tropospheric concentration of O$_3$, OH, CO, CH$_4$ and NO$_x$, *Tellus, 39B*, 271-285, 1987.

Jacob, D.J., and S.C. Wofsy, Photochemistry of biogenic emissions over the Amazon forest, *J. Geophys. Res., 93*, 1477-1486, 1988.

Jacob, D.J, and S.C. Wofsy, Budgets of reactive nitrogen, hydrocarbons, and ozone over the Amazon forest during the wet season, *J. Geophys. Res., 95*, 16,737-16,744, 1990.

Jacob, D.J., et al., Summertime photochemistry of the troposphere at high northern latitudes, *J. Geophys. Res., 97*, 16,421-16,431, 1992.

Jacob, D.J., et al., Simulation of summertime ozone over North America, *J. Geophys. Res., 98*, 14,797-14,816, 1993.

Kasibhatla, P.S., H. Levy II, and W.J. Moxim, Global NO$_x$, HNO$_3$, PAN, and NO$_y$ distributions from fossil fuel combustion emissions: A model study, *J. Geophys. Res., 98*, 7165-7180, 1993.

Kelly, T.J., D.H. Stedman, J.A. Ritter, and R.B. Harvey, Measurements of oxides of nitrogen and nitric acid in clean air, *J. Geophys. Res., 85*, 7417-7425, 1980.

Klinger, L.F., P.R. Zimmermann, J.P. Greenberg, L.E. Heidt, and A.B. Guenther, Carbon trace gas fluxes along a successional gradient in the Hudson Bay lowland, *J. Geophys. Res., 99*, 1469-1494, 1994.

Lamb, R.G., W.H. Chen, and J.H. Seinfeld, Numerico-empirical analyses of atmospheric diffusion theories, *J. Atmos. Sci., 32*, 1794-1807, 1975.

Levy II, H., and W.J. Moxim, Fate of US and Canadian combustion nitrogen emissions, *Nature, 328*, 414-416, 1987.

Liu, S.C., et al., A study of the photochemistry and ozone budget during the Mauna Loa Observatory Photochemistry Experiment, *J. Geophys. Res., 97*, 10,463-10,471, 1992.

Logan, J.A., M.J. Prather, S.C. Wofsy, and M.B. McElroy, Tropospheric chemistry: A global perspective, *J. Geophys. Res., 86*, 7210-7254, 1981.

Lurmann, F.W., A.C. Lloyd, and R. Atkinson, A chemical mechanism for use in long-range transport/acid deposition computer modeling, *J. Geophys. Res., 91*, 10,905-10,936, 1986.

Madronich, S., Intercomparison of NO$_2$ photodissociation and U.V. radiometer measurements, *Atmos. Environ., 21*, 569-578, 1987.

Madronich, S., and J.G. Calvert, Permutation reactions of organic peroxy radicals in the troposphere, *J. Geophys. Res., 95*, 5697-5715, 1990.

Mozurkewich, M., and J.G. Calvert, Reaction probability of N$_2$O$_5$ on aqueous aerosols, *J. Geophys. Res., 93*, 15,889-15,896, 1988.

Parrish, D.D., M. Trainer, E.J. Williams, D.W. Fahey, G. Hübler, C.S. Eubank, S.C. Liu, P.C. Murphy, D.L. Albritton, and F.C. Fehsenfeld, Measurements of the NO$_x$-O$_3$ photostationary state at Niwot Ridge, Colorado, *J. Geophys. Res., 91*, 5361-5370, 1986.

Paulson, S.E., and J.H. Seinfeld, Development and evaluation of a photochemical mechanism for isoprene, *J. Geophys. Res., 97*, 20,703-20,715, 1992.

Penner, J.E., C.S. Atherton, J. Dignon, S.J. Ghan, J.J. Walton, and S. Hameed, Tropospheric nitrogen: A three-dimensional study of sources, distributions, and deposition, *J. Geophys. Res., 96*, 959-990, 1991.

Ridley, B.A., M.A. Carroll, A.L. Torres, E.P. Condon, G.W. Sachse, G.F. Hill, and G.L. Gregory, An intercomparison of results from ferrous sulfate and photolytic converter techniques for measurements of NO$_x$ made during the NASA GTE CITE 1 aircraft program, *J. Geophys. Res., 93*, 15,803-15,811, 1988.

Ridley, B.A., S. Madronich, R.B. Chatfield, J.G. Walega, R.E. Shetter, M.A. Carroll, and D.D. Montzka, Measurements and model simulations of the photostationary state during the Mauna Loa Observatory Photochemistry Experiment: Implications for radical concentrations and ozone production and loss rates, *J. Geophys. Res., 97*, 10,375-10,388, 1992.

Ritter, J.A., D.H. Stedman, and T.J. Kelly, Ground-level measurements of nitric oxide, nitrogen dioxide, and ozone in rural air, in *Nitrogenous Air Pollutants: Chemical and Biological Implications*, edited by D. Grojean, Butterworth, Stoneham, Mass., 1979.

Sandholm, S.T., et al., Summertime tropospheric observations related to N$_x$O$_y$ distributions and partitioning over Alaska: Arctic Boundary Layer Expedition 3A, *J. Geophys. Res., 97*, 16,481-16,510, 1992.

Sandholm, S., et al., Summertime partitioning and budget of NO$_y$ compounds in the troposphere over Alaska and Canada: ABLE 3B, *J. Geophys. Res., 99*, 1837-1861, 1994.

Shetter, R.E., A.H. McDaniel, C.A. Cantrell, S. Madronich, and J.G. Calvert, Actinometer and Eppley radiometer measurements of the NO$_2$ photolysis rate coefficient during the Mauna Loa Observatory Photochemistry Experiment, *J. Geophys. Res., 97*, 10,349-10,359, 1992.

Shipham, M.C., A.S. Backmeier, D.R. Cahoon Jr., G.L. Gregory, B. E. Anderson, and E.V. Browell, A meteorological interpretation of the Atmospheric Boundary Layer Expedition (ABLE) 3B flight series, *J. Geophys. Res., 99*, 1645-1657, 1994.

Singh, H.B., and P.L. Hanst, Peroxyacetyl nitrate (PAN) in the unpolluted atmosphere: An important reservoir for nitrogen oxides, *Geophys. Res. Lett., 8*, 941-944, 1981.

Singh, H.B., L.J. Salas, and W. Viezee, The global distribution of peroxyacetyl nitrate, *Nature, 321*, 588-591, 1986.

Singh, H.B., et al., Peroxyacetyl nitrate measurements during CITE 2: Atmospheric distribution and precursor relationships, *J. Geophys. Res., 95*, 10,163-10,178, 1990.

Singh, H.B., D. O'Hara, D. Herlth, J.D. Bradshaw, S.T. Sandholm, G.L. Gregory, G.W. Sachse, D.R. Blake, P.J. Crutzen, and M.A. Kanakidou, Atmospheric measurements of peroxyacetyl nitrate and other organic nitrates at high latitudes: Possible sources and sinks, *J. Geophys. Res., 97*, 16,511-16,522, 1992.

Singh, H.B., et al., Summertime distribution of PAN and other reactive nitrogen species in the northern high latitude atmosphere of eastern Canada, *J. Geophys. Res., 99*, 1821-1835, 1994a.

Singh, H.B., D. O'Hara, D. Herlth, W. Sachse, D.R. Blake, J.D. Bradshaw, M. Kanakidou, and P.J. Crutzen, Acetone in the atmosphere: Distribution, sources and sinks, *J. Geophys. Res., 99*, 1805-1819, 1994b.

Talbot, R.W., et al., Summertime distribution and relations of reactive nitrogen species and NO$_y$ in the troposphere over Canada, *J. Geophys. Res., 99*, 1863-1885, 1994.

Tang, I.N., H.R. Munkelwitz, and J.G. Davis, Aerosol growth studies, IV, Phase transformation of mixed salt aerosols in a moist atmosphere, *J. Aerosol Sci., 9*, 505-511, 1978.

Thompson, A.M., The oxidizing capacity of the Earth's atmosphere: Probable past and future changes, *Science, 256*, 1157-1165, 1992.

Trainer, M., E.Y. Hsie, S.A. McKeen, R. Tallamraju, D.D. Parrish, F.C. Fehsenfeld, and S.C. Liu, Impact of natural hydrocarbons on hydroxyl and peroxy radicals, *J. Geophys. Res., 92,* 11,879-11,894, 1987.

Trainer, M., et al., Observations and modeling of the reactive nitrogen photochemistry at a rural site, *J. Geophys. Res., 96,* 3045-3064, 1991.

Travagli, G., L'etere dinitrico del metilenglicol, *Gazz. Chim. Ital., 68,* 718-721, 1938.

Tuazon, E.C., and R. Atkinson, A product study of the gas-phase reaction of methyl vinyl ketone with the OH radical in the presence of NO$_x$, *Internat. J. Chem. Kinet., 21,* 1141-1152, 1989.

Tuazon, E.C., and R. Atkinson, A product study of the gas-phase reaction of methacrolein with the OH radical in the presence of NO$_x$, *Internat. J. Chem. Kinet., 22,* 591-602, 1990a.

Tuazon, E.C., and R. Atkinson, A product study of the gas-phase reaction of isoprene with the OH radical in the presence of NO$_x$, *Internat. J. Chem. Kinet., 22,* 1221-1236, 1990b.

Volz, A., D. Mihelcic, P. Musigen, H.W. Patz, G. Pilwat, H. Geiss, and D. Kley, Ozone production in the Black Forest: Direct measurements of RO$_2$, NO$_x$ and other relevant parameters, in *NATO Workshop on Tropospheric Ozone: Regional and Global Ozone and Its Environmental Consequences,* edited by I.S.A. Isaksen, pp. 293-302, D. Reidel, Norwell, Mass., 1988.

Walega, J.G., B.A. Ridley, S. Madronich, F.E. Grahek, J.D. Shetter, T.D. Sauvain, C.J. Hahn, J.T. Merill, B.A. Bodhaine, and E. Robinson, Observations of peroxyacetyl nitrate, peroxypropionyl nitrate, methyl nitrate, and ozone during the Mauna Loa Observatory Photochemistry Experiment, *J. Geophys. Res., 97,* 10,311-10,330, 1992.

Wofsy, S.C., S.-M. Fan, D.R. Blake, J.D. Bradshaw, S.T. Sandholm, H.B. Singh, G.W. Sachse, and R.C. Harriss, Factors influencing atmospheric composition over subarctic North America during summer, *J. Geophys. Res., 99,* 1887-1897, 1994.

D. R. Blake, Department of Chemistry, University of California, Irvine, CA 92171.

J. D. Bradshaw and S. T. Sandholm, School of Earth and Atmospheric Sciences, Georgia Institute of Technology, Atlanta, GA 30332.

S.-M. Fan, D. J. Jacob, and D. L. Mauzerall, Division of Applied Sciences, Harvard University, Cambridge, MA 02138.

G. L. Gregory and G. W. Sachse, NASA Langley Research Center, Hampton, VA 22331.

H. B. Singh, NASA Ames Research Center, Moffett Field, 94305.

R. W. Talbot, Complex Systems Research Center, University of New Hampshire, Durham, NH 03814.